DOI: 10.1111/cgf.14900
Eurographics Symposium on Geometry Processing 2023
P. Memari and J. Solomon
(Guest Editors)

COMPUTER GRAPHICS *forum*
Volume 42 (2023), Number 5
e14900 *pp. 1 - 11*

Quadratic-Attraction Subdivision

K. Karčiauskas[1] and J. Peters[2]

[1]Vilnius University
[2] University of Florida

Abstract

The idea of improving multi-sided piecewise polynomial surfaces, by explicitly prescribing their behavior at a central surface point, allows for decoupling shape finding from enforcing local smoothness constraints. Quadratic-Attraction Subdivision determines the completion of a quadratic expansion at the central point to attract a differentiable subdivision surface towards bounded curvature, with good shape also in-the-large.

CCS Concepts

• ***Computing methodologies*** → ***Parametric curve and surface models;*** • ***Mathematics of computing*** → ***Continuous functions;***

1. Introduction

Classical subdivision algorithms, and Catmull-Clark subdivision in particular, have found widespread acceptance due to their intuitive simplicity of generalizing uniform knot insertion of B-splines as local mesh refinement. At extraordinary points, classical subdivision can be expressed as multiplication with a sparse matrix. A series of optimizations ('tuning') that use of larger footprint rules have been proposed to address shape problems near the extraordinary point. Guided Subdivision harnesses a larger number of degrees of freedom by first computing a fixed surface prototype from the control net. The prototype surface is called the guide. A refinement step can then be viewed as adding an inner surface ring to a nested sequence of rings whose limit converges to the guide. A more recent class of 'point-augmented' subdivision (PAS) algorithms aims to combine the simplicity of classical algorithms with the observed good shape of guided subdivision: PAS surfaces exhibit considerably better curvature distribution than optimized classical algorithms, both in-the-large and in the vicinity of the extraordinary point – but, like classical algorithms, can still be implemented as repeated matrix multiplication. However, PAS algorithms are not curvature bounded. (C^2 continuity would require increased degree of the surface rings [PR08, Chap 6].) Tuned algorithms achieve bounded curvature, but ostensibly at the price of oscillating curvature. This raises the question whether low-degree matrix-based algorithms can be both curvature-bounded and deliver good shape?

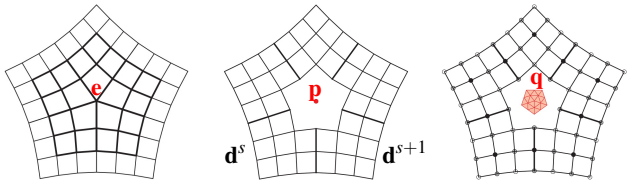

(a) **c**-*net* **(b)** *PAS:* **d**-*net* + **p** **(c)** *QAS*$^{\square}$*:* **d**-*net* + **q**

Figure 1: *Evolution of control nets (a)* **c***-net (thick lines) for Catmull-Clark subdivision (CC) (b)* 12*n nodes of the* **d***-net and a point* **p** *define Point-Augmented Subdivision (PAS) (c) A* **d***-net and the attracting quadratic* **q** *define the shape of Quadratic-Attraction Subdivision (QAS*$^{\square}$*).*

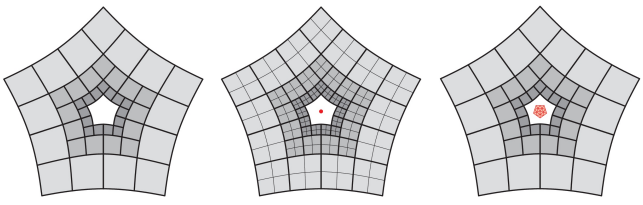

(a) *CC* **(b)** *PAS*^{3} + **p** **(c)** *QAS*^{4} + **q**

Figure 2: *Contracting sequences of surface rings generated from the input of Fig. 1. (a)* 3*n bicubic (bi-3) pieces per ring; (b)* 12*n bi-3 pieces (c)* 3*n bi-4 pieces.*

The contribution of this paper is to show that a generalization of the PAS-approach yields all three desiderata for, by choice, either bicubic (bi-3) or biquartic (bi-4) subdivision surfaces. Moreover, the rules have a smaller footprint and yield increased flexibility at the central point. Nevertheless, the control net can remain the same as for PAS algorithms with only the augmenting point **p** replaced

by a quadratic expansion **q** and different formulas. Honoring its ancestor, the new approach is called Quadratic-Attraction Subdivision abbreviated as QAS$^{\square}$. (The $\square$ serves to disambiguate from [BS07] which generates an everywhere piecewise total degree 3-sided quadratic approximation to Loop subdivision [Cha87].) Remarkably, the derivation of QAS$^{\square}$ shows an alternative derivation of visually identical variants of the PAS algorithms, all in a common framework. These relations are summarized in Fig. 12. Besides guaranteeing bounded curvature, the freedom in setting **q** yields higher flexibility at the central point (see Fig. 14). This benefits applications, not elaborated here, ranging from Hermite interpolation to solving differential equations.

Overview Section 2 gives a focused review of the relevant subdivision algorithms. Section 3 prepares some basic technical tools. Section 4 presents curvature-bounded QAS^4 subdivision and Section 5 its limit analysis. Section 6 derives a curvature-bounded bi-cubic QAS^3 from QAS^4. Section 7 explains how the refinement rules of additional PAS-like algorithms are obtained from QAS$^{\square}$ algorithms. Section 8 compares the resulting subdivision surfaces.

2. Subdivision Surface Synopsis

We focus on linear and uniform subdivision algorithms, the class to which the QAS$^{\square}$-algorithms belong. The two subsections review classical and guided subdivision algorithms, and the recent Point-Augmented (PAS) algorithms.

2.1. Classical and guided subdivision algorithms

Subdivision surface algorithms can be viewed as generating a sequence of contracting surface rings, see Fig. 2, by refining a control net and interpreting the nodes of the net as weights of basis functions. Classical subdivision surfaces, like Catmull-Clark subdivision [CC78], are controlled by a **c**-net, see Fig. 1a: an extraordinary node **e** at the center is irregular, i.e. has fewer or more than the regular $n = 4$ neighbors, and is surrounded by layers of the quadrilateral facets, a.k.a. quads. All internal nodes other than **e** are regular and define bicubic (bi-3) surface pieces; the outermost nodes can be irregular. Correspondingly, except for the extraordinary node, all nodes are refined by uniform bi-3 B-spline knot-insertion rules. Requiring just one special rule for each extraordinary node simplifies implementation [NLMD12]. However, the simple rules often result in unwanted non-uniformly distributed highlight lines [BC94] near the limit of the extraordinary node, the extraordinary point.

Subdivision tuning [Sab91] aims to better control curvature at the extraordinary point by adjusting the eigenexpansion of the linear subdivision rules. For example, [MM18] provides carefully chosen rules not just for the extraordinary node but also for its $2n$ nearest neighbors and replaces each bi-3 patch of Catmull-Clark subdivision by 2×2 bi-3 macro-patches. The resulting shape is improved and the curvature is bounded, but highlight lines oscillate at the transitions between the surface rings, see also [PU98]. Another example of tuning, [LFS16] prescribes a part of the Taylor expansion explicitly to address unequal spacing.

Guided Subdivision [KP07, KP18, KP19] may be viewed as prescribing a limit shape at the central point **p** via an initially-computed guide surface. Empirically, guided subdivision results in very good highlight line distribution, but implementation requires to first construct the guide surface and then sample it to complete the contracting rings.

2.2. Point-Augmented Subdivision (PAS^d)

The idea of improving the construction of multi-, non-four-sided surface configurations, by explicitly prescribing their behavior at a central surface point, has been explored repeatedly [Pra97, Lev06, KP18]. The approach may be viewed as smartly mixing interpolation and approximation where n pieces come together at an extraordinary point. However, leaving the description of the limit behavior to the designer is skirting the main challenge of how to, as a default and automatically, set those degrees of freedom to achieve good shape. Moreover, providing a separate interface for manipulation of each n-sided neighborhood yields a complex implementation and wielding it may be impractical for large objects. Even when set automatically, as for Guided Subdivision, separate data structures complicate the implementation and downstream use. The recently proposed Point-Augmented Subdivision, abbreviated as PAS^3 for the bi-cubic version [KP23c] and PAS^4 for its better-shaped bi-quartic relative [KP23a], have therefore aimed to replicate the good surface shape of the guide by baking the guide construction into the subdivision rules. The contracting control net neighborhood of each extraordinary point, when multiplying the net with a subdivision matrix, provides nested subdivision surface rings. Remarkably, PAS^3 and PAS^4 match the surface quality of Guided Subdivision while formulated as explicit formulas familiar from classical or tuned algorithms.

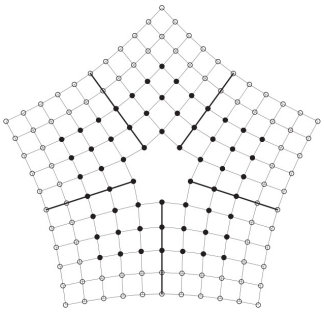

Figure 3: *PAS^3: **c**-net $\rightarrow$ **d**-net.*

Point-augmented subdivision, PAS^3 refines a **d**-net consisting of $12n$ nodes plus a central fixed point **p**, see Fig. 1b. If the input is a **c**-net. the **d**-net is derived by regular bi-cubic refinement (uniform knot insertion) of the eligible parts of the **c**-net, as illustrated in Fig. 3: the $12n$ • of the **d**-net are derived from the thick subnet in Fig. 1a. Notably, PAS^3 preserves the second-order Hermite data defined by the **d**-net and therefore of any original **c**-net, whereas various tuned algorithms (e.g. [MM18]), do not preserve the second order data. A sector of each ring consists of three 2×2 bi-3 macro-patches, see Fig. 2b. The $6n$ refined nodes marked as • in Fig. 4a have special rules, but rotational and sector-diagonal symmetries reduce the number of distinct rules to five. Although five special rules is more than Catmull-Clark (one) and the best tuned, [MM18] (three), the rules are *explicit* and operate directly on input data. While delivering highlight lines akin to Guided Subdivision that make the surface essentially better than Catmull-Clark and [MM18], structurally PAS^3 is therefore simpler than Guided Subdivision. The key to this good shape is a piecewise polynomial guide baked into the PAS^3 rules. The baked-in guide *changes*

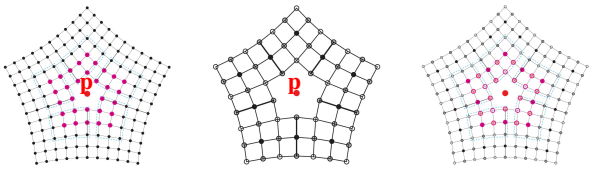

(a) *PAS*^{3} *refinement* **(b)** *PAS*^{4}*:* **d***-net+* **p** **(c)** *PAS*^{4} *refinement*

Figure 4: *PAS refinement of a* **d***-net. (a) PAS*^{3} *defines* $6n$ *new nodes, marked* •*, by special rules that take into account the augmenting point* **p***; the remaining nodes are obtained by regular bi-cubic refinement (knot insertion). (b)* $12n$ *nodes of the* **d***-net corresponding to uniform* C^2 *bi-4 spline refinement. (c) PAS*^{4} *refinement:* $6n$ *magenta nodes* • *are defined by special rules and* **p***; the remaining nodes are obtained via regular* C^2 *bi-4 refinement (knot insertion).*

for each refinement step. That is, in contrast to guided subdivision where the guide is explicitly constructed and static, these evolving guides have been computed *symbolically* as a formula from which the refinement rules have been derived. Since they are baked-in, the existence of the guides can be ignored for implementation as a matrix multiplication. The curvature of PAS^3 at the limit point **p** is nominally unbounded but increases slowly.

In PAS^4 [KP23a] each sector of the contracting ring consists of only three (not twelve) bi-4 patches, but the number of nodes, connectivity of **d**-net and augmentation look like PAS^3: compare Fig. 4c vs Fig. 4a. The essential difference is that the nodes of **d**-net are, just as for QAS^4, interpreted as C^2 bi-4 B-spline coefficients. For these uniform C^2 bi-4 (B-)splines, tensoring the single variable case leads to three types of nodes illustrated in Fig. 4b and corresponding to: simple knots in both directions (marked as ○); double knots in both directions (marked as •); a simple knot in one and a double knot in the other direction, marked as the circled gray bullets.

3. Preliminaries and Building Blocks

The subdivision surface rings consist of tensor-product patches of degree bi-d in Bernstein-Bézier form (BB-form, [dB87,Far88]): for Bernstein polynomials $B_k^d(t) := \binom{d}{k}(1-t)^{d-k}t^k$,

$$\mathbf{p}(u,v) := \sum_{i=0}^{d}\sum_{j=0}^{d} \mathbf{p}_{ij} B_i^d(u) B_j^d(v), \quad 0 \le u,v \le 1.$$

The *BB-coefficients* $\mathbf{p}_{ij} \in \mathbb{R}^3$ are connected to $\mathbf{p}_{i+1,j}$ and $\mathbf{p}_{i,j+1}$ wherever possible and this forms the *BB-net*.

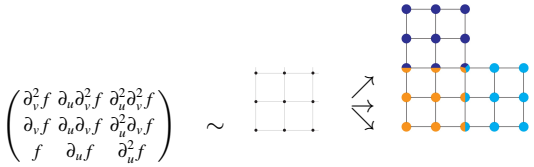

Figure 5: *Three corner jets (rotated by* $\pi/2$ *for* • *and* $-\pi/2$ *for* • *so that the corner BB-coefficient is* f *evaluated at the corresponding corner of the unit square) assembled into an L-net of degree bi-4.*

The construction repeatedly uses Taylor expansions or *jets* in BB-form, at corners of patches and along boundaries of patches, called *tensor-borders*. For example, the second-order Taylor expansion of a map f at a corner of its unit square domain can be collected in the matrix of partial derivatives at a corner point, see Fig. 5, *left*, that is re-expressed as a 3×3 BB-net (*right* of $\sim$) of some degree bi-d. Three corner jets (cyan, orange and blue) of degree bi-4 can be merged into an L-net by averaging the BB-coefficients at overlapping locations.

In order to derive bi-3 PAS^3 and QAS^3 subdivision from their corresponding bi-4 algorithms PAS^4 and QAS^4, we recall the well-known change of basis from B-spline to BB-form (B-to-BB),see [KP23a, Eq. 6] for bi-4 C^2 splines. Fig. 6 shows the bijection

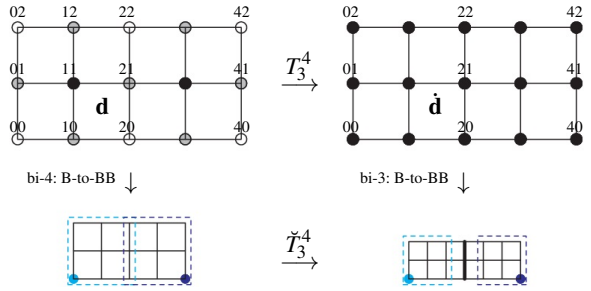

Figure 6: *Transformation* T_3^4*:* $\mathbf{d} \to \dot{\mathbf{d}}$.

T_3^4 between the net $\mathbf{d}$ of the bi-4 constructions and net $\dot{\mathbf{d}}$ of the bi-3 constructions via the invertible tensor-border transformation $\check{T}_3^4$, preceded by the bi-4 B-to-BB conversion and followed by the inverse bi-3 B-to-BB conversion. In more detail, the bi-4 tensor-border Fig. 6, *bottom,left* is evenly split and its 3×3 corner jets at the cyan and blue corner points are presented in bi-3 form, see Fig. 6, *bottom,right*. The corner jets in bi-3 form are then joined C^1 by setting the BB-coefficients of the thick line as averages of their horizontal neighbors. Remarkably, this bi-3 tensor-border is C^2. By construction, $\check{T}_3^4$ preserves the 3×3 corner jets at cyan and blue corners. We can explicitly state T_3^4 and its inverse:

$$\begin{aligned}
\dot{\mathbf{d}}_{ij} &:= \mathbf{d}_{ij},\ i=0,2,\ j=0,2;\\
\dot{\mathbf{d}}_{i1} &:= \frac{1}{8}[1,6,1]\,[\mathbf{d}_{i0},\mathbf{d}_{i1},\mathbf{d}_{i2}]^T, i=0,2;\\
\dot{\mathbf{d}}_{ij} &:= \frac{1}{8}[1,6,1]\,[\mathbf{d}_{i-1,j},\mathbf{d}_{ij},\mathbf{d}_{i+1,j}]^T, i=1,j=0,2;\\
\dot{\mathbf{d}}_{i1} &:= \frac{1}{64}[1,6,1,6,36,6,1,6,1]\,\mathbf{D}_i,\ i=1,\\
\mathbf{D}_i &:= [\mathbf{d}_{i-1,0},\mathbf{d}_{i0},\mathbf{d}_{i+1,0},\mathbf{d}_{i-1,1},\mathbf{d}_{i1},\mathbf{d}_{i+1,1},\mathbf{d}_{i-1,2},\mathbf{d}_{i2},\mathbf{d}_{i+1,2}]^T.
\end{aligned} \tag{T_3^4}$$

$$\begin{aligned}
\mathbf{d}_{ij} &:= \dot{\mathbf{d}}_{ij},\ i=0,2,\ j=0,2;\\
\mathbf{d}_{i1} &:= \frac{1}{6}[-1,8,-1]\,[\dot{\mathbf{d}}_{i0},\dot{\mathbf{d}}_{i1},\dot{\mathbf{d}}_{i2}]^T, i=0,2;\\
\mathbf{d}_{ij} &:= \frac{1}{6}[-1,8,-1]\,[\dot{\mathbf{d}}_{i-1,j},\dot{\mathbf{d}}_{ij},\dot{\mathbf{d}}_{i+1,j}]^T, i=1,j=0,2;\\
\mathbf{d}_{i1} &:= \frac{1}{36}[1,-8,1,-8,64,-8,1,-8,1]\,\dot{\mathbf{D}}_i,\ i=1,
\end{aligned} \tag{$(T_3^4)^{-1}$}$$

$\dot{\mathbf{D}}_i := [\dot{\mathbf{d}}_{i-1,0},\dot{\mathbf{d}}_{i0},\dot{\mathbf{d}}_{i+1,0},\dot{\mathbf{d}}_{i-1,1},\dot{\mathbf{d}}_{i1},\dot{\mathbf{d}}_{i+1,1},\dot{\mathbf{d}}_{i-1,2},\dot{\mathbf{d}}_{i2},\dot{\mathbf{d}}_{i+1,2}]^T$.
Both formulas have a 'shift by 2' symmetry: in $\dot{\mathbf{d}}_{rs}$, $r,s=0,1,2$, replacing the $\mathbf{d}_{ij}$ by $\mathbf{d}_{i+2,j}$, $i,j=0,1,2$, yields $\dot{\mathbf{d}}_{r+2,s}$; in $\mathbf{d}_{rs}$,

$r,s = 0,1,2$, replacing the $\dot{\mathbf{d}}_{ij}$ by $\dot{\mathbf{d}}_{i+2,j}$, $i,j = 0,1,2$, we get $\mathbf{d}_{r+2,s}$. It suffices to describe T_3^4 and $(T_3^4)^{-1}$ on one 3×3 dark-gray and one light-gray sub-net shown in Fig. 7 since their formulas are symmetric with respect to $i=1$ and $j=1$ and diagonal flip.

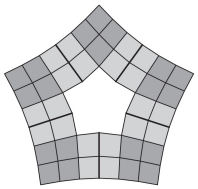

Figure 7: $\mathbf{d} \leftrightarrow \dot{\mathbf{d}}$.

4. Degree bi-4 Quadratic-Attraction Subdivision: QAS^4

To be integrated into the QAS^4 refinement rules, high-quality guides must be derived symbolically. We use the **d**-net-labels displayed in Fig. 8a (a copy of Fig. 1c) and look at Fig. 8b for the refined structure. We focus on the initialization of the quadratic **q** in Section 4.2 since the refinement, reviewed in Section 4.1, is akin to [KP23a] and [KP23c]. The explicit formulas of the refined net in terms of the input net, and the complete QAS^4-Algorithm are then stated in Section 4.3.

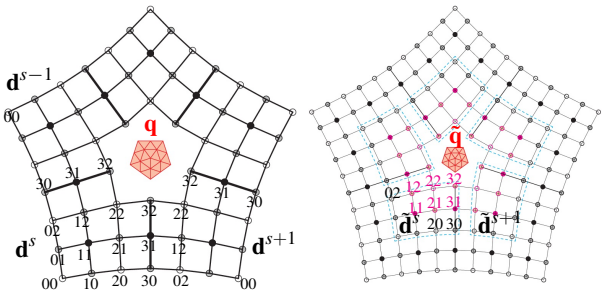

(a) *QAS^4:* **d***-net +* **q** **(b)** *QAS^4 refinement*

Figure 8: *(a) Labels of the* **d***-net. (b) The nodes marked as* •, ∘ *and the circled* • *are obtained from* **d***-net via regular C^2 bi-4 refinement. In each sector s, the* 12 *refined nodes of* $\tilde{\mathbf{d}}^s$ *are surrounded by dashed cyan lines.*

4.1. Derivation of the refinement step $(\mathbf{d},\mathbf{q}) \to (\tilde{\mathbf{d}},\tilde{\mathbf{q}})$

Fig. 9a shows the bi-4 tensor-border in BB-form, with L-shaped sectors, obtained by applying B-to-BB conversion to the **d**-net. Fig. 9b shows the BB-net of an intermediate map $\mathbf{g}^{\triangle}$ of total degree 5 [Far88, Ch.17]. The map is piecewise C^1, has a unique quadratic expansion **q** at the central point **p** that is determined, for example, by the 6 coefficients of the first sector $\mathbf{q}_i^0$, $i=1,\dots,6$, where $\mathbf{q}_1^0 := \mathbf{p}$. Setting for $s = 1,\dots,n-1$,

$$\begin{pmatrix} \mathbf{q}_1^{s+1} \\ \mathbf{q}_2^{s+1} \\ \mathbf{q}_3^{s+1} \\ \mathbf{q}_4^{s+1} \\ \mathbf{q}_5^{s+1} \\ \mathbf{q}_6^{s+1} \end{pmatrix} := A \begin{pmatrix} \mathbf{q}_1^{s} \\ \mathbf{q}_2^{s} \\ \mathbf{q}_3^{s} \\ \mathbf{q}_4^{s} \\ \mathbf{q}_5^{s} \\ \mathbf{q}_6^{s} \end{pmatrix}, \quad A := \begin{pmatrix} 1 & 0 & 0 & 0 & 0 & 0 \\ 0 & 0 & 0 & 1 & 0 & 0 \\ 0 & 0 & 0 & 0 & 0 & 0 \\ 2(1-\mathsf{c}) & -1 & 0 & 2\mathsf{c} & 0 & 0 \\ 0 & 0 & 0 & 2(1-\mathsf{c}) & -1 & 2\mathsf{c} \\ 4(1-\mathsf{c})^2 & 4(1-\mathsf{c}) & 1 & 8\mathsf{c}(1-\mathsf{c}) & -4\mathsf{c} & 4\mathsf{c}^2 \end{pmatrix}, \tag{1}$$

where $\mathsf{c} := \cos(2\pi/n)$, defines the remaining sectors. For refinement, the domain of **q** is scaled down, towards the origin, by the subdominant eigenvalue λ of Catmull-Clark subdivision. This

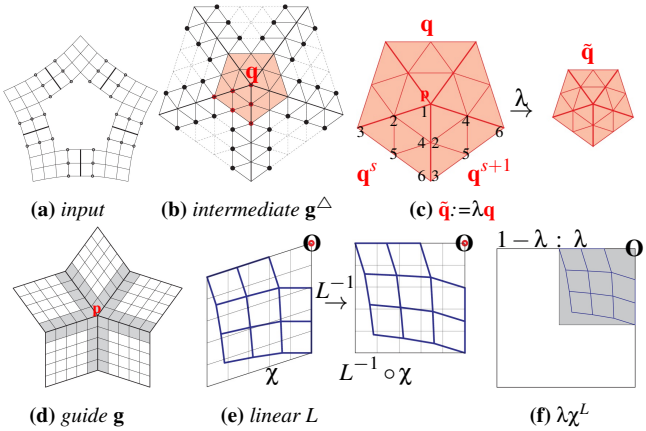

(a) *input* **(b)** *intermediate* $\mathbf{g}^{\triangle}$ **(c)** $\tilde{\mathbf{q}}:=\lambda\mathbf{q}$

(d) *guide* **g** **(e)** *linear L* **(f)** $\lambda\chi^L$

Figure 9: *Guide and refinement derivation steps. (e,f)* **O** *denotes the origin in* $\mathbb{R}^2$. *(b) The relevant (active) points of the intermediate guide* $\mathbf{g}^{\triangle}$ *are joined by solid lines.*

yields $\tilde{\mathbf{q}}$, the restriction of **q** to the down-scaled domain:

$$\begin{pmatrix} \tilde{\mathbf{q}}_1^s \\ \tilde{\mathbf{q}}_2^s \\ \tilde{\mathbf{q}}_3^s \\ \tilde{\mathbf{q}}_4^s \\ \tilde{\mathbf{q}}_5^s \\ \tilde{\mathbf{q}}_6^s \end{pmatrix} := S \begin{pmatrix} \mathbf{q}_1^s \\ \mathbf{q}_2^s \\ \mathbf{q}_3^s \\ \mathbf{q}_4^s \\ \mathbf{q}_5^s \\ \mathbf{q}_6^s \end{pmatrix}, \; S := \begin{pmatrix} 1 & 0 & 0 & 0 & 0 & 0 \\ 1-\lambda & \lambda & 0 & 0 & 0 & 0 \\ (1-\lambda)^2 & 2(1-\lambda)\lambda & \lambda^2 & 0 & 0 & 0 \\ 1-\lambda & 0 & 0 & \lambda & 0 & 0 \\ (1-\lambda)^2 & (1-\lambda)\lambda & 0 & (1-\lambda)\lambda & \lambda^2 & 0 \\ (1-\lambda)^2 & 0 & 0 & 2(1-\lambda)\lambda & 0 & \lambda^2 \end{pmatrix}. \tag{2}$$

Fig. 9d shows the increase of degrees of freedom when the domain of $\mathbf{g}^{\triangle}$ is mapped, by composition, to multiple parallelograms to form a piecewise bi-5 G^1 map **g** as follows. The linear shear map L of Fig. 9e transforms the unit square into a unit parallelogram with opening angle $\frac{2\pi}{n}$. Piecewise composition with L implies that the gray-underlaid BB-coefficients of **g** determine the same Hermite data as the total degree Bézier points of $\mathbf{g}^{\triangle}$ joined by solid lines. Then **g** is sampled with $L^{-1}\circ\chi$ to create one sector of tensor-borders; the unmarked $16n$ BB-coefficients are unknown (free) and set to match the 3×3 corner jets of input tensor-border. Remarkably, although $16n > 9n$, all degrees of freedom can be pinned-down without loss of quality, i.e. the guide **g** captures well the second-order Hermite data of input tensor-border. Summarizing this part of the derivation, the BB-coefficients of **g** are expressed via the nodes of the input **d**-net plus 6 coefficients $\mathbf{q}_i^0$, $i=1,\dots,6$ that determine the quadratic expansion **q**.

Fig. 9f shows the restriction of sector $\mathbf{g}^s$ to the λ-down-scaled domain. Sampling the jets at corner locations of $\lambda L^{-1}\circ\chi$ results in L-shaped C^2 bi-4 tensor-borders. These tensor-borders are re-expressed by BB-to-B conversion (see Section 3) as the refined nodes $\tilde{\mathbf{d}}_{ij}^s$, $i=1,2,3$, $j=1,2$ (• in Fig. 8b). The remaining 6 nodes $\tilde{\mathbf{d}}_{i0}^s$, $i=0,\dots,3$, $\tilde{\mathbf{d}}_{0j}^s$, $j=1,2$, are obtained by regular refinement of **d**. Without sacrificing good shape, we can truncate the resulting linear map $(\mathbf{d},\mathbf{q}) \to (\tilde{\mathbf{d}},\tilde{\mathbf{q}})$ to 5 digits after the decimal point (as was done in [KP23c, KP23a]) and list all entries scaled by 10^5 as integers. The Appendix presents the corresponding integer matrices K and T for valencies $n=3,5,\dots,10$.

4.2. Initializing q from the d-net

The choice of $\mathbf{q}$ is important to achieve high QAS^4 surface quality. With the bi-5 guide $\mathbf{g}$ determined in Section 4.1, the 5 coefficients $\mathbf{q}_i^0$, $i=2,\dots,6$, are set to minimize the functional

$$\mathcal{F}_k f := \int_0^1 \int_0^1 \sum_{i+j=k,i,j\geq 0} \frac{k!}{i!\,j!}(\partial_s^i \partial_t^j f(s,t))^2 \, ds\, dt\,, \qquad (3)$$

for $k=5$, over all n bi-5 sectors of $\mathbf{g}$. The central point $\mathbf{q}_1^s := \mathbf{p}$, $s=0,\dots,n-1$, is set as in [KP23a, Eq. 3] for a $\mathbf{c}$-net and [KP23a, Eq. 4] for a $\mathbf{d}$-net input. Truncation of $\mathbf{q}$ to 5 digits after the decimal point and scaling by 10^5 yields a compact listing as integers, but results in a quadratic expansion defined only with 10^{-5} accuracy and approximate curvature-boundedness.

An exact quadratic expansion $\mathbf{q}$ is obtained by computing, for each sector r, a slightly different proposal $\bar{\mathbf{q}}^{r,0}$ using the truncated pre-calculated weights. The $\bar{\mathbf{q}}^{r,0}$ are C^0 connected and require only small corrections to satisfy the C^1 and the C^2 constraints. Each propose a similar quadratic expansion. (This freedom of proposals can also be used for design, see Fig. 14.) Given $\bar{\mathbf{q}}_i^{r,0}$, $i=1,\dots,6$, $r=0,\dots,n-1$ satisfying $\bar{\mathbf{q}}_1^{r,0} := \mathbf{p}$, $\bar{\mathbf{q}}_2^{r+1,0} := \bar{\mathbf{q}}_4^{r,0}$, $\bar{\mathbf{q}}_3^{r+1,0} := \bar{\mathbf{q}}_6^{r,0}$, the following two steps re-establish an exact quadratic expansion $\mathbf{q}$:

- For each r and $s=1,\dots,n-1$, formula (1) defines

$$(\bar{\mathbf{q}}_1^{r,s}\dots\bar{\mathbf{q}}_6^{r,s})^T := A(\bar{\mathbf{q}}_1^{r,s-1}\dots\bar{\mathbf{q}}_6^{r,s-1})^T\,. \qquad (4)$$

- For $s=0,\dots,n-1$, set $\mathbf{q}_1^s := \mathbf{p}$ and compute

$$\mathbf{q}_k^s := \frac{1}{n}\sum_{r=0}^{n-1} \bar{\mathbf{q}}_k^{s-r,r},\ k=2,\dots,6\,. \qquad (5)$$

We summarize how to **compute a unique q from the truncated formulas**:
(S1) Set the central point $\mathbf{q}_1^s := \mathbf{p}$, $s=0,\dots,n-1$, as in [KP23a, Eq. 3] for a $\mathbf{c}$-net and [KP23a, Eq. 4] for a $\mathbf{d}$-net input.
(S2) For each valence n and $k=4,5$, let $\bar{Q}^k := Q_n^k$. For $i=0,\dots,3$, $j=0,1,2$, $s=0,\dots,n-1$, set

$$\mu_{ij}^{k,s} := 10^{-5}\bar{Q}^k_{s+1,1+4j+i} \text{ and } \dot{\mu}^k := 1-\sum_{s=0}^{n-1}\sum_{j=0}^{2}\sum_{i=0}^{3}\mu_{ij}^{k,s}\,.$$

For $r=0,\dots,n-1$, set $\bar{\mathbf{q}}_1^{r,0} := \mathbf{p}$, and for $k=4,5$,

$$\bar{\mathbf{q}}_k^{r,0} := \sum_{s=0}^{n-1}\sum_{j=0}^{2}\sum_{i=0}^{3}\mu_{ij}^{k,s}\mathbf{d}_{ij}^{r+s} + \dot{\mu}^k\mathbf{p};\quad \bar{\mathbf{q}}_2^{r+1,0} := \bar{\mathbf{q}}_4^{r,0};$$
$$\bar{\mathbf{q}}_6^{r,0} := \frac{1}{2\mathsf{c}}\left(\bar{\mathbf{q}}_5^{r,0} + \bar{\mathbf{q}}_5^{r+1,0} - 2(1-\mathsf{c})\bar{\mathbf{q}}_4^{r,0}\right),\quad \bar{\mathbf{q}}_3^{r+1,0} := \bar{\mathbf{q}}_6^{r,0}\,.$$

(S3) Apply formulas (4), (5).

4.3. Explicit formulas of the refined net: $\tilde{\mathbf{d}}_{ij}^s$, $i=1,2,3$, $j=1,2$

With κ from the tables K and τ from tables T in the Appendix, for $i=1,2$, $j=1,2$, and $s=0,\dots,n-1$:

$$\tilde{\mathbf{d}}_{ij}^s := \sum_{r=-1}^{1}\sum_{m=0}^{2}\sum_{l=0}^{3}\kappa_{lm}^s\mathbf{d}_{lm}^{s+r} + \sum_{k=2}^{6}\tau_{ij,k}\mathbf{q}_k^s + (1-\sum_{r=-1}^{1}\sum_{m=0}^{2}\sum_{l=0}^{3}\kappa_{lm}^s - \sum_{k=2}^{6}\tau_{ij,k})\mathbf{p}, \qquad (6)$$

For $i=3$, $j=1,2$, and $s=0,\dots,n-1$:

$$\tilde{\mathbf{d}}_{3j}^s := \sum_{r=-1}^{2}\sum_{m=0}^{2}\sum_{l=0}^{3}\kappa_{lm}^s\mathbf{d}_{lm}^{s+r} + \frac{1}{2}\sum_{k=2}^{6}\tau_{3j,k}\mathbf{q}_k^s + \frac{1}{2}\big(\tau_{3j,2}\mathbf{q}_4^{s+1} + \tau_{3j,3}\mathbf{q}_6^{s+1} + \tau_{3j,4}\mathbf{q}_2^{s+1} + \tau_{3j,5}\mathbf{q}_5^{s+1} + \tau_{3j,6}\mathbf{q}_3^{s+1}\big) + (1-\sum_{r=-1}^{2}\sum_{m=0}^{2}\sum_{l=0}^{3}\kappa_{lm}^s - \sum_{k=2}^{6}\tau_{3j,k})\mathbf{p}\,. \qquad (7)$$

We summarize:

QAS^4 Algorithm

1. If the input is a $\mathbf{c}$-net, convert it to a $\mathbf{d}$-net as in [KP23a, Fig. 5] and set $\mathbf{q}_1^s := \mathbf{p}$, $s=0,\dots,n-1$ by [KP23a, Eq. 3]; else set $\mathbf{p}$ by [KP23a, Eq. 4].
2. Compute $\mathbf{q}$ by (S1), (S2), (S3).
3. Iterate
   a. Refine the $\mathbf{d}$-net to $\tilde{\mathbf{d}}$ (Fig. 8b): compute $24n$ nodes marked •, ○ and • by uniform bi-4 C^2 spline knot insertion; compute $6n$ nodes • by (6) and (7).
   b. Define $\tilde{\mathbf{q}}$ from $\mathbf{q}$ by formula (2).
   c. Update $\tilde{\mathbf{q}}\to\mathbf{q}$ and $\tilde{\mathbf{d}}\to\mathbf{d}$.
   d. B-to-BB convert the $30n$ refined nodes to $3n$ bi-4 patches forming a new surface ring as in Fig. 2c.

See [PLK] for an implementation.

5. Limit analysis

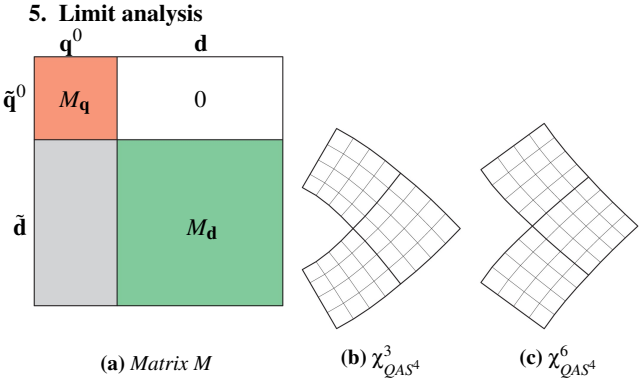

(a) *Matrix M* **(b)** $\chi^3_{QAS^4}$ **(c)** $\chi^6_{QAS^4}$

Figure 10: *(a) Structure of the subdivision matrix M. (b,c) One sector of the characteristic map of QAS^4 for $n=3$ and for $n=6$.*

The $(12n+6)\times(12n+6)$ subdivision matrix M splits into four submatrices, see Fig. 10a, of which one has zero entries. $M_{\mathbf{q}}$ is

equal to matrix S in (2) whose eigenvalues are $1,\lambda,\lambda,\lambda^2,\lambda^2,\lambda^2$. Numerical calculation shows that all eigenvalues of $M_{\mathbf{d}}$ to be less than λ^2 in absolute value. Therefore QAS^4 is curvature bounded. Visually almost identical to [KP23a, Fig 9], the BB-nets of the characteristic map $n = 3,5,\ldots,10$, look very similar to (but are not identical to) the degree-raised characteristic maps of Catmull-Clark subdivision, see Fig. 10b,c. Numerical computation confirms positivity of $\partial_u \chi^n_{\mathrm{QAS}^4} \times \partial_v \chi^n_{\mathrm{QAS}^4}$ for $n = 3,5,\ldots,10$, i.e. injectivity of the QAS^4 characteristic map for valencies $n = 3,5,\ldots,10$.

6. Degree bi-3 Quadratic-Attraction Subdivision: QAS^3

QAS^3 has the same net structure as QAS^4, cf. Fig. 11 and Fig. 8. However, the QAS^3 nodes $\dot{\mathbf{d}}$ are interpreted as control points of C^2 bi-3 splines rather than C^2 bi-4 splines. T_3^4 and $(T_3^4)^{-1}$ of Section 3 transform technical operations from QAS^4 to QAS^3, see Steps 2, 3a below.

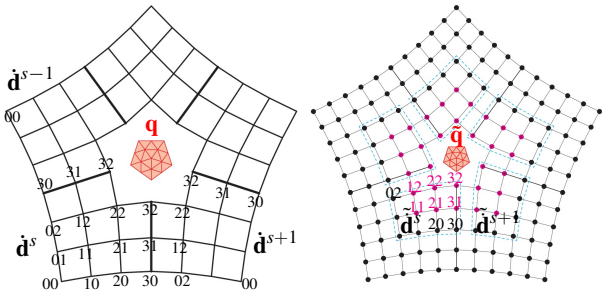

(a) *QAS^3:* **d***-net +* **q** **(b)** *QAS^3 refinement*

Figure 11: *(a) Labeling of* $\dot{\mathbf{d}}$*-net. (b)* $30n$ *refined nodes: the inner* $12n$ *form the refined net* $\tilde{\mathbf{d}}$*. The outer nodes marked as* • *are obtained from* $\dot{\mathbf{d}}$*-net via regular* C^2 *bi-3 refinement, while the* • *are defined by the special rules.*

QAS^3 Algorithm

1. If the input is a **c**-net, convert it to a $\dot{\mathbf{d}}$-net as in Fig. 3 and set $\mathbf{q}_1^s := \mathbf{p}$, $s = 0,\ldots,n-1$ by [KP23c, Eq.(1)]; else set $\mathbf{p}$ by [KP23c, Eq.(2)].
2. Apply $(T_3^4)^{-1}$ to express $\mathbf{d}$ in terms of $\dot{\mathbf{d}}$. Then compute $\mathbf{q}$ according to Section 4.2.
3. Iterate
   a. Refine the $\dot{\mathbf{d}}$-net (Fig. 11): compute the $24n$ nodes marked • in Fig. 11b by uniform bi-3 spline knot insertion; for the $6n$ •, apply $(T_3^4)^{-1}$ to be able to use formulas (6) and (7) in terms of $\dot{\mathbf{d}}$, and apply T_3^4 to transform the result back from $\tilde{\mathbf{d}}$ to $\tilde{\dot{\mathbf{d}}}$.
   b. Define $\tilde{\mathbf{q}}$ from $\mathbf{q}$ by formula (2).
   c. Update $\tilde{\mathbf{q}} \to \mathbf{q}$ and $\tilde{\dot{\mathbf{d}}} \to \dot{\mathbf{d}}$.
   d. B-to-BB convert the $30n$ refined nodes to $12n$ bi-3 pieces forming a new surface ring of 2×2 macro-patches as in Fig. 2b.

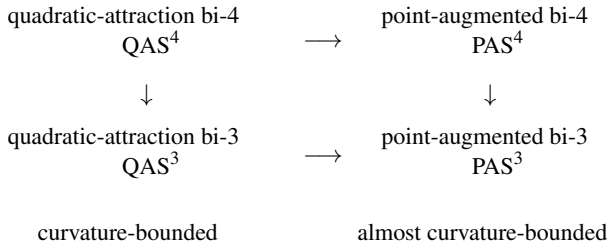

Figure 12: *Genealogy of the subdivision algorithms presented in this paper.*

Remark. One can reduce the arithmetic operations in 3a by deriving expressions of refined nodes $\tilde{\dot{\mathbf{d}}}^s_{ij}$ explicitly in terms of $(\dot{\mathbf{d}}, \mathbf{p})$.

Limit analysis Since the submatrix $M_{\mathbf{q}}$ is the same as for QAS^4 (cf. Fig. 10), its dominating eigenvalues in the QAS^3 matrix imply curvature-boundedness. The BB-nets of the characteristic maps are visually very similar to those of Catmull-Clark subdivision, when its bi-3 patches are split into 2×2 pieces. The injectivity of QAS^3 characteristic map has been verified by numerical computation.

7. Alternative PAS algorithms

From the QAS$^{\square}$- algorithms we can derive PAS-type subdivision algorithms that differ only slightly from [KP23a] and [KP23c]. Together this yields the academically satisfying unified derivation illustrated in Fig. 12. The main difference in the **d**-net refinement rules for QAS^4 vs PAS^4 [KP23a] lies in the λ-scaled sampling of the guide **g**, displayed in Fig. 9f. In QAS^4, the BB-coefficients of **g** are expressed via the nodes of input **d**-net plus 6 coefficients $\mathbf{q}_1^0 := \mathbf{p}$, $\mathbf{q}_i^0$, $i = 2,\ldots,6$. In PAS^4, the expressions (5) are substituted for $\mathbf{q}_i^0$, $i = 2,\ldots,6$, retaining only a symbolic **p**, so that the BB-coefficients of **g** are expressed via the nodes of the input **d**-net and **p**. Then, formulas (6) and (7) complete the refinement step.

Analogously, the $\dot{\mathbf{d}}$-net refinement rules for PAS^3 follow from QAS^3 by expressing the BB-coefficients of **g** in terms of the $\dot{\mathbf{d}}$-net plus an undetermined central point **p** and substituting into formulas of refined nodes $\dot{\mathbf{d}}$ derived by Step 3a of the *QAS^3* algorithm.

The refinement rules of the new PAS^4 and PAS^3 are similar to those in [KP23a] and [KP23c] and yield surfaces of comparable quality, see Section 8. They differ in that [KP23a] and [KP23c] minimize $\mathcal{F}_4$, while the unified derivation minimizes $\mathcal{F}_5$. If instead $\mathcal{F}_4$ is minimized, the observed differences are negligible for $n = 3,5,6$ and the surfaces are like twins. But, due to truncation, for $n = 8,9,10$ the surface quality of the unified PAS^4 and PAS^3 suffer when $\mathcal{F}_4$ is minimized, see Fig. 13.

8. Discussion and Examples

In the hope that enforcing bounded curvature constraints will improve shape, tuned subdivision, e.g. [MM18], has worked hard with the full net of $12n+1$ nodes displayed in Fig. 1a to find rules that tame the additional degrees of freedom. In [MM18] new rules are

ultimately applied only to the $2n$ nodes nearest the extraordinary node. [KP23c] pioneered the idea of introducing a sequence of guide surfaces directly into the refinement formulas. This has the advantage that new refinement rules can be defined for $6n$ nodes of the **d**-net while supporting predictable design of shape.

But first, we demonstrate, in Fig. 13, the difference between applying $\mathcal{F}_4$ vs $\mathcal{F}_5$ for high valences n, and convex input. The $n = 10$ sectors in Fig. 13a are planar. The top row of Fig. 13 shows (b) a surrounding green bi-3 surface and the red subdivision surface and (c) the artifact-free transition from one to the other (typical for all schemes derived in this paper). The views from the top, in rows 2 and 3, zoom in on the first 8 rings so as to just fit into the red subdivision region. The red and cyan lines in (e) point to the oscillations in the highlight lines of (d), compared to applying $\mathcal{F}_5$ in (f). Where do these oscillation originate? (g) and (h) show them to be 'first step artifacts': applying $\mathcal{F}_4$ once and then $\mathcal{F}_5$ yields strong oscillations compared to one step of $\mathcal{F}_5$ followed by $\mathcal{F}_4$. Clearly just focusing on the limit for shape tuning is not a good strategy. The highlight lines of the two *bottom* rows are taken so close to the limit point as to be irrelevant for most applications, yet confirm that the careful guide construction for bounded curvature also pays off in the limit.

The reduction in highlight line oscillations is not the main improvement of QAS^4 over PAS^4. Fig. 14 illustrates a key advantage of Quadratic-Attraction of QAS^4 over PAS^4: **q** can be modified as a whole in the spirit of moving a group of NURBS nodes for design. For example, we apply an affine transformation to the default initial **q**. Additionally, one can vary individual points of the quadratic expansion, noting that this requires the post-treatment (4) and (5) of Section 4.2 to ensure a unique quadratic expansion. Note the increased expressiveness of (e) QAS^4 over (g) PAS^4. This allows for better approximation both in the geometry and any functions on the geometry expressed in terms of QAS$^\square$. Fig. 14c,d illustrate good shape of the default QAS^4 surfaces. A variety of strong modifications of **q** are handled well by QAS^4, see in (g-n). By contrast, for PAS^4 only the point **p** can be modified, restricting the design options. Analogous modifications can of course be applied to the corresponding bi-3 subdivision surfaces.

Fig. 15 *top* row applies PAS^4 to an input mesh containing tightly packed irregular nodes of valence $n = 3,5,6$. For these valencies, the new PAS^4 surfaces are visually very similar to those of [KP23a]. Fig. 15 *bottom* row applies PAS^3. The resulting surfaces are very similar to the ones generated by [KP23c].

Fig. 16 compares 8 rings of various subdivision surfaces for a low valence, yet challenging input. While the highlight lines of conventional and tuned subdivision algorithms [CC78, MM18, WM23] oscillate those of QAS^3 are calm. PAS^3 highlight lines look identical even in Gauss curvature shading. The point of this example is that PAS^3 does not formally guarantee bounded-curvature, while [MM18, WM23] do. Yet, as with earlier tuned versions of Catmull-Clark subdivision, the theoretically superior quality at the extraordinary point results in undesirable oscillations. Thanks to the guided approach, despite formally unbounded curvature, PAS yields a calm highlight line distribution. QAS$^\square$ retains, and even slightly improves, the highlight line distribution, achieves bounded curvature, an advance in subdivision theory, has more local refinement rules and offers increased flexibility at the center.

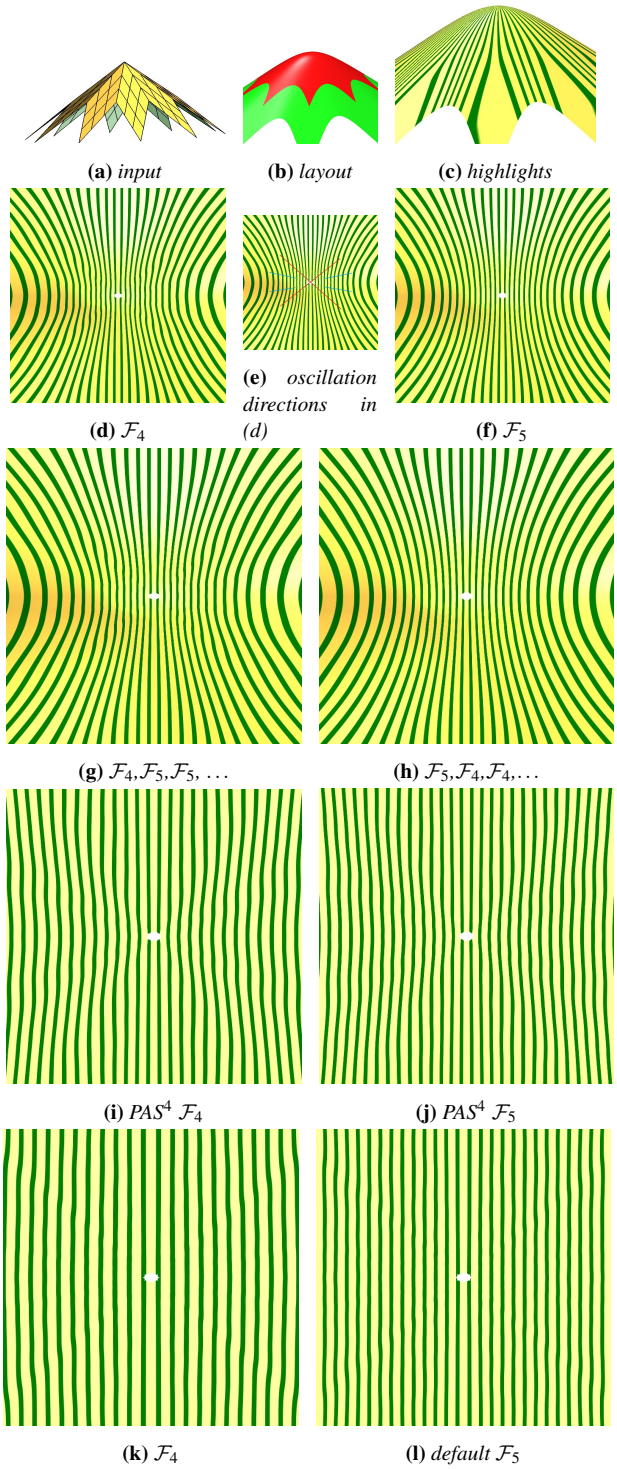

Figure 13: *Discussion of functionals for a convex shape, $n = 10$. All surfaces except (i) and (j) are generated using QAS^4. (d) – (h) show bi-4 rings $1,\ldots,8$. (i) – (l) show rings $8,\ldots,15$. That is, the shape difference to PAS^4 is minute.*

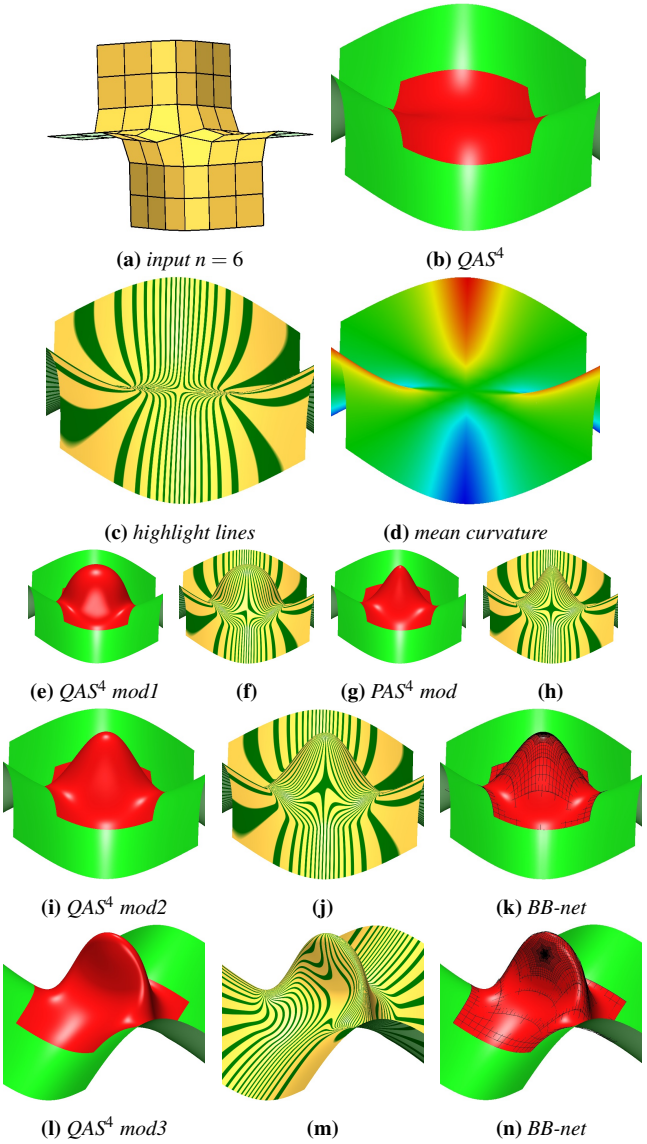

Figure 14: *Quadratic flexibility of QAS$^{\square}$ illustrated by three modifications of* **q** *of the monkey saddle.*

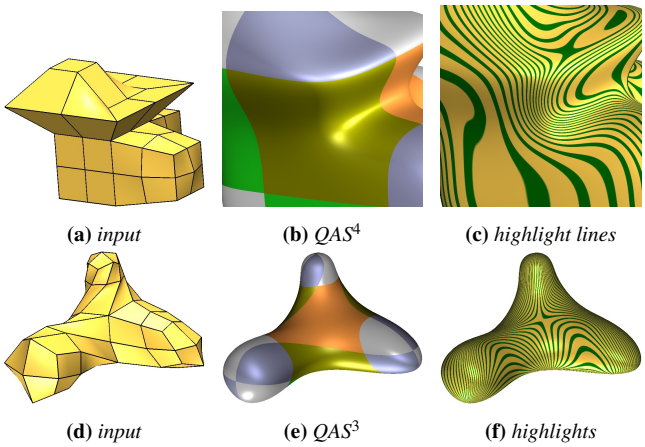

Figure 15: *Two meshes with node valencies $n = 3,5,6$. (b,c) zoom.*

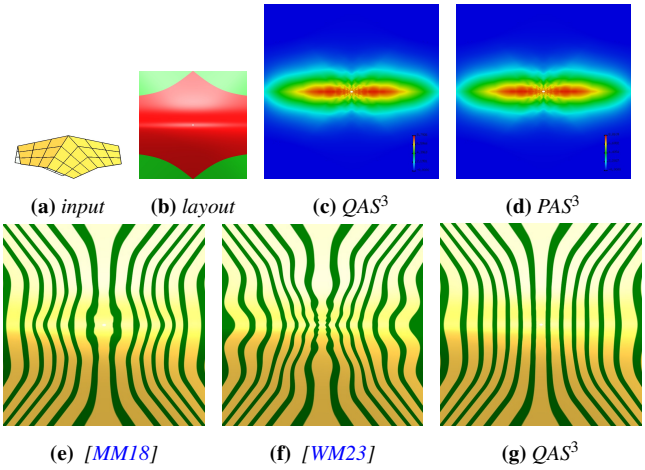

Figure 16: *(a) Convex input with $n = 6$ flat 3×3 facets outlining a parabolic shape. (b) bi-3 input ring and contracting rings; (c,d) Gauss curvature in range $[0..0.79]$ for QAS^3 and $[0..0.81]$ for PAS^3; (e,f,g) highlight lines.*

Fig. 17 compares 12 rings of bi-3 subdivision surfaces for $n = 9$. Again the highlight lines exhibit oscillations for [MM19] and [WM23] but not for QAS^3 – with default initialization of **q** and therefore almost identically shaped to its sibling PAS^3. The curvature distributions of QAS^3 and PAS^3 are visually very similar: even after 12 refinement steps, the curvatures, although unbounded for PAS^3, are barely growing.

The cost for QAS$^{\square}$ or PAS subdivision is only slightly higher than for Catmull-Clark subdivision or its tuned variants [MM18, WM23]. If we treat sectors of **q** as independent with a common central point **p**, then the QAS$^{\square}$ control net has $5n$ more nodes than the $12n+1$ nodes forming the control nets of all other subdivision algorithms considered in this paper. The proportion of zeros in the subdivision matrices increases with the valence, $n = 3,5,\ldots,10$. The percentage of zeros is [84..95] for [CC78, MM18, WM23], [43..46] for PAS and [72..91] for QAS$^{\square}$. Implementing QAS$^{\square}$ in lieu of Catmull-Clark only requires switching out the subdivision matrix and initializing **d** from the **c**-net and, if wanted, a default **q** from **d** by applying a matrix of size $5n \times (12n+1)$. (Implementing the subdivision step-by-step as explained in Section 4, instead of assembling the matrix, requires less storage, but all matrix sizes are small for modern computers.)

Limitations We assume that the input is a quad mesh and that any quad has at most one extraordinary node. One midpoint refinement, e.g. [CC78], can convert inadmissible quad meshes to such an input. For any polyhedral mesh two steps guarantee separation.

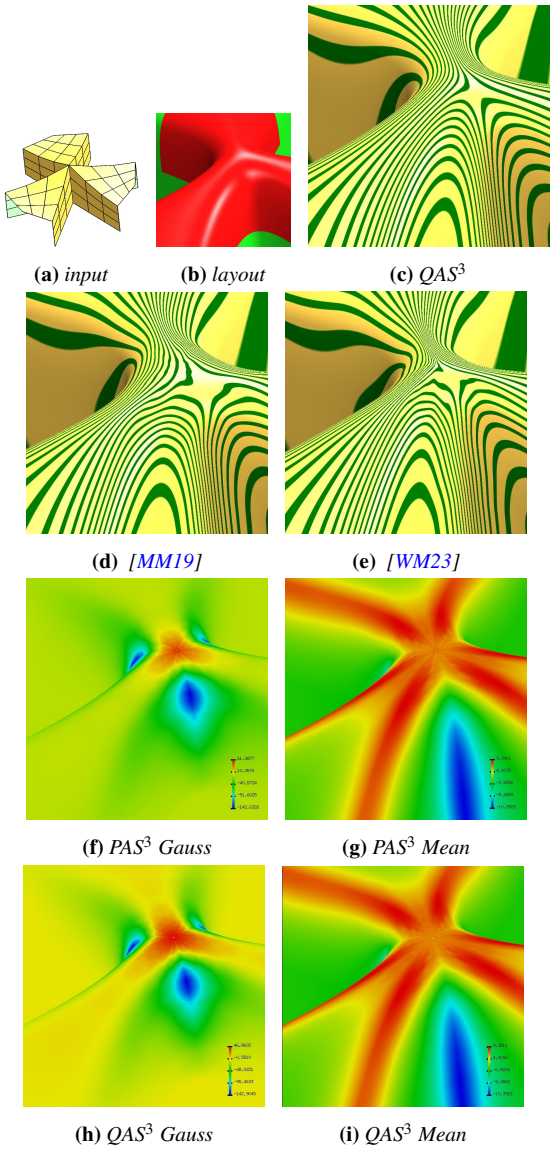

(a) *input* **(b)** *layout* **(c)** *QAS*^{3}

(d) *[MM19]* **(e)** *[WM23]*

(f) *PAS*^{3} *Gauss* **(g)** *PAS*^{3} *Mean*

(h) *QAS*^{3} *Gauss* **(i)** *QAS*^{3} *Mean*

Figure 17: *(a) Challenging high-valence $n = 9$ net, yielding the surface in (b). (c,d,e) highlight lines; (g,i) Mean curvature with range $[-10..9]$. (f,h) Gauss curvature with range $[-143..k]$, where $k = 47$ for QAS^3 and $k = 61$ for PAS^3.*

9. Conclusion

The new family of attracting algorithms generate the refined net by a linear process. Therefore the subdivision matrix, see Fig. 10a, can be used for fast evaluation in the spirit of Sabin and Stam [DS78, Sta98]. For the implementation, the (non-regular) Catmull-Clark subdivision rules can be replaced by any of the QAS$^\square$ or PAS algorithms, see the implementation of QAS^4 at [PLK]. Grafting QAS^4 onto a bi-cubic tensor-product spline body preserves high-end quality, but uniformity of degree may give QAS^3 an edge. While the guide principle in their derivation makes PAS surfaces look similar to QAS$^\square$, QAS$^\square$has several advantages: higher flexibility at the central point, bounded curvature and rules with a more localized footprint.

Since infinite refinement is not practical, if the finest resolution, for example to avoid pixel dropout at the extraordinary points, is not known, one can cover the remaining hole with a tiny piecewise smooth bi-4, respectively bi-3 cap construction from the literature, e.g. [KP23b].

Acknowledgments

The work was supported, in part, by a donation from AMD.

References

[BC94] BEIER K.-P., CHEN Y.: Highlight-line algorithm for realtime surface-quality assessment. *Comp-Aid Design 26*, 4 (1994), 268–277. 2

[BS07] BOUBEKEUR T., SCHLICK C.: QAS: Real-time quadratic approximation of subdivision surfaces. In *15th Pacific Conference on Computer Graphics and Applications (PG'07)* (2007), IEEE, pp. 453–456. 2

[CC78] CATMULL E., CLARK J.: Recursively generated B-spline surfaces on arbitrary topological meshes. *Computer-Aided Design 10* (Sept. 1978), 350–355. 2, 7, 8

[Cha87] CHARLES T. L.: Smooth subdivision surfaces based on triangles. *M. S Thesis, The University of Utah* (1987). 2

[dB87] DE BOOR C.: B-form basics. In *Geometric Modeling: Algorithms and New Trends* (1987), Farin G., (Ed.), SIAM, pp. 131–148. 3

[DS78] DOO D., SABIN M.: Behaviour of recursive division surfaces near extraordinary points. *Computer-Aided Design 10* (Sept. 1978), 356–360. 9

[Far88] FARIN G.: *Curves and Surfaces for Computer Aided Geometric Design: A Practical Guide*. Academic Press, 1988. 3, 4

[KP07] KARČIAUSKAS K., PETERS J.: Concentric tesselation maps and curvature continuous guided surfaces. *Computer Aided Geometric Design 24*, 2 (Feb 2007), 99–111. 2

[KP18] KARČIAUSKAS K., PETERS J.: Refinable bi-quartics for design and analysis. *Computer-Aided Design* (2018), 1–10. 2

[KP19] KARČIAUSKAS K., PETERS J.: Curvature-bounded guided subdivision: biquartics vs bicubics. *Computer Aided Design* (Jul 2019), 1–11. 2

[KP23a] KARČIAUSKAS K., PETERS J.: Evolving guide subdivision. vol. 42, Wiley, pp. 321–332. Eurographics 2023. 2, 3, 4, 5, 6, 7

[KP23b] KARČIAUSKAS K., PETERS J.: Improved caps for improved subdivision surfaces. *Computer-Aided Design* (2023), 103543. 9

[KP23c] KARČIAUSKAS K., PETERS J.: Point-augmented bi-cubic subdivision surfaces. *Computer Graphics Forum 41*, 7 (March 2023), 13–23. 2, 4, 6, 7

[Lev06] LEVIN A.: Modified subdivision surfaces with continuous curvature. In *ACM SIGGRAPH 2006 Papers*. 2006, pp. 1035–1040. 2

[LFS16] LI X., FINNIGAN G., SEDERBERG T.: G^1 non-uniform Catmull-Clark surfaces. *ACM Transactions on Graphics 35* (07 2016), 1–8. 2

[MM18] MA Y., MA W.: Subdivision schemes with optimal bounded curvature near extraordinary vertices. *Computer Graphics Forum 37*, 7 (Oct 2018), 455–467. 2, 6, 7, 8

[MM19] MA Y., MA W.: Subdivision schemes for quadrilateral meshes with the least polar artifact in extraordinary regions. *Comput. Graph. Forum 38*, 7 (2019), 127–139. 8, 9

[NLMD12] NIESSNER M., LOOP C., MEYER M., DEROSE T.: Feature-adaptive gpu rendering of catmull-clark subdivision surfaces. *ACM Transactions on Graphics (TOG) 31*, 1 (2012), 1–11. 2

[PLK] PETERS J., LO K., KARČIAUSKAS K.: Quadratic-attraction subdivision, C++ code. https://bitbucket.org/surflab/quadratic-attraction-subdivision. 5, 9

[PR08] PETERS J., REIF U.: *Subdivision Surfaces*, vol. 3 of *Geometry and Computing*. Springer-Verlag, New York, 2008. 1

[Pra97] PRAUTZSCH H.: Freeform splines. *Comput. Aided Geom. Des 14*, 3 (1997). 2

[PU98] PRAUTZSCH H., UMLAUF G.: A G^2-subdivision algorithm. In *Geometric Modelling*. Springer, 1998, pp. 217–224. 2

[Sab91] SABIN M. A.: Cubic recursive division with bounded curvature. In *Curves and surfaces*. Elsevier, 1991, pp. 411–414. 2

[Sta98] STAM J.: Exact evaluation of Catmull-Clark subdivision surfaces at arbitrary parameter values. In *Proceedings of the 25th annual conference on Computer graphics and interactive techniques* (1998), pp. 395–404. 9

[WM23] WANG X., MA W.: An extended tuned subdivision scheme with optimal convergence for isogeometric analysis. *Computer-Aided Design* (2023), 103544. 7, 8, 9

Appendix: Q_n^k for computing q

The tables Q_n^4 and Q_n^5 define the weights

$$\mu_{ij}^{k,s} := 10^{-5}\bar{Q}^k_{s+1,1+4j+i},\ i=0,1,2,3,\ j=0,1,2,s=0,\dots,n-1,$$

for each valence n, $k=4,5$ and $\bar{Q}^k := Q_n^k$ in (S2) of Section 4.2:

$$Q_3^4 := \begin{pmatrix} 0 & 0 & -22 & -60 & 6 & -28 & 699 & 2395 & -16 & 388 & 3837 & 8400 \\ 0 & 6 & -16 & 30 & 0 & -28 & 388 & -1197 & -22 & 699 & 3837 & -4200 \\ 1 & -7 & 39 & 30 & -7 & 56 & -1087 & -1197 & 39 & -1087 & -7675 & -4200 \end{pmatrix}$$

$$Q_3^5 := \begin{pmatrix} -2 & 18 & -63 & -101 & 18 & -116 & 1214 & -130 & -63 & 1214 & 7588 & 451 \\ 1 & -3 & 40 & 148 & -12 & 61 & -409 & -2289 & 4 & -2259 & -8664 & -9186 \\ 1 & -12 & 4 & -101 & -3 & 61 & -2259 & -130 & 40 & -409 & -8664 & 451 \end{pmatrix}$$

$$Q_5^4 := \begin{pmatrix} -69 & 2 & 190 & 2 & 18 & 757 & -1491 & -701 & 184 & -1535 & 6707 & 9114 \\ -69 & 18 & 184 & 0 & 2 & 757 & -1535 & -216 & 190 & -1491 & 6707 & 2816 \\ 26 & 9 & -76 & -1 & -16 & -289 & 542 & 567 & -67 & 613 & -2562 & -7373 \\ 86 & -12 & -231 & -1 & -12 & -936 & 1871 & 567 & -231 & 1871 & -8291 & -7373 \\ 26 & -16 & -67 & 0 & 9 & -289 & 613 & -216 & -76 & 542 & -2562 & 2816 \end{pmatrix}$$

$$Q_5^5 := \begin{pmatrix} -297 & 186 & 640 & 55 & 186 & 2555 & -6144 & -1242 & 640 & -6144 & 24879 & 16601 \\ 29 & 41 & -223 & 51 & -4 & -460 & 1151 & 1041 & -123 & 899 & -681 & -10803 \\ 42 & 101 & -186 & 49 & 81 & -936 & 940 & 185 & -314 & 1603 & -5611 & -3330 \\ 42 & 81 & -314 & 51 & 101 & -936 & 1603 & 1041 & -186 & 940 & -5611 & -10803 \\ 29 & -4 & -123 & 55 & 41 & -460 & 899 & -1242 & -223 & 1151 & -681 & 16601 \end{pmatrix}$$

$$Q_6^4 := \begin{pmatrix} 581 & -1583 & 1173 & 88 & -1405 & 2604 & -742 & -4346 & 1130 & -1255 & 3747 & 11992 \\ 581 & -1405 & 1130 & 44 & -1583 & 2604 & -1255 & -2173 & 1173 & -742 & 3747 & 5996 \\ 0 & 178 & -43 & -44 & -178 & 0 & -512 & 2173 & 43 & 512 & 0 & -5996 \\ -581 & 1583 & -1173 & -88 & 1405 & -2604 & 742 & 4346 & -1130 & 1255 & -3747 & -11992 \\ -581 & 1405 & -1130 & -44 & 1583 & -2604 & 1255 & 2173 & -1173 & 742 & -3747 & -5996 \\ 0 & -178 & 43 & 44 & 178 & 0 & 512 & -2173 & -43 & -512 & 0 & 5996 \end{pmatrix}$$

$$Q_6^5 := \begin{pmatrix} 1219 & -3600 & 3395 & 236 & -3600 & 8000 & -6249 & -9577 & 3395 & -6249 & 19545 & 28052 \\ 1220 & -1928 & 778 & 487 & -3028 & 2522 & 746 & -515 & 1679 & 2178 & 364 & -5816 \\ 56 & 494 & -754 & -30 & 525 & -2686 & 2638 & 3461 & -1395 & 4281 & -7131 & -7925 \\ -1108 & 2377 & -1213 & -30 & 2377 & -2417 & -2253 & 3461 & -1213 & -2253 & 4553 & -7925 \\ 56 & 525 & -1395 & 487 & 494 & -2686 & 4281 & -515 & -754 & 2638 & -7131 & -5816 \\ 1220 & -3028 & 1679 & 236 & -1928 & 2522 & 2178 & -9577 & 778 & 746 & 364 & 28052 \end{pmatrix}$$

$$Q_7^4 := \begin{pmatrix} 2101 & -4029 & 1523 & 1626 & -3828 & 3082 & 3263 & -11053 & 1657 & 2657 & -944 & 14900 \\ 2101 & -3828 & 1657 & 1014 & -4029 & 3082 & 2657 & -6891 & 1523 & 3263 & -944 & 9290 \\ 519 & -745 & 543 & -361 & -1195 & 761 & 50 & 2459 & 242 & 1412 & -233 & -3315 \\ -1454 & 2899 & -980 & -1465 & 2538 & -2133 & -2594 & 9959 & -1221 & -1502 & 653 & -13425 \\ -2332 & 4360 & -1765 & -1465 & 4360 & -3421 & -3285 & 9959 & -1765 & -3285 & 1048 & -13425 \\ -1454 & 2538 & -1221 & -361 & 2899 & -2133 & -1502 & 2459 & -980 & -2594 & 653 & -3315 \\ 519 & -1195 & 242 & 1014 & -745 & 761 & 1412 & -6891 & 543 & 50 & -233 & 9290 \end{pmatrix}$$

$$Q_7^5 := \begin{pmatrix} 6832 & -12914 & 5811 & 4146 & -12914 & 10981 & 6990 & -28695 & 5811 & 6990 & 2219 & 40625 \\ 3858 & -5871 & 1962 & 1548 & -7821 & 4329 & 5353 & -5201 & 2414 & 8373 & -2988 & 580 \\ -470 & 1643 & -1380 & -659 & 1411 & -3290 & 2028 & 7207 & -2317 & 4014 & -4675 & -12420 \\ -1586 & 2639 & -506 & -1273 & 3321 & -2071 & -3741 & 6703 & -1459 & -3492 & 3987 & -5024 \\ -1586 & 3321 & -1459 & -659 & 2639 & -2071 & -3492 & 7207 & -506 & -3741 & 3987 & -12420 \\ -470 & 1411 & -2317 & 1548 & 1643 & -3290 & 4014 & -5201 & -1380 & 2028 & -4675 & 580 \\ 3858 & -7821 & 2414 & 4146 & -5871 & 4329 & 8373 & -28695 & 1962 & 5353 & -2988 & 40625 \end{pmatrix}$$

$$Q_8^4 := \begin{pmatrix} 2967 & -4866 & 916 & 3172 & -4728 & 1818 & 6117 & -14457 & 1124 & 5769 & -2534 & 14544 \\ 2967 & -4728 & 1124 & 2243 & -4866 & 1818 & 5769 & -10222 & 916 & 6117 & -2534 & 10284 \\ 1229 & -1820 & 674 & 0 & -2154 & 753 & 2041 & 0 & 171 & 2882 & -1049 & 0 \\ -1229 & 2154 & -171 & -2243 & 1820 & -753 & -2882 & 10222 & -674 & -2041 & 1049 & -10284 \\ -2967 & 4866 & -916 & -3172 & 4728 & -1818 & -6117 & 14457 & -1124 & -5769 & 2534 & -14544 \\ -2967 & 4728 & -1124 & -2243 & 4866 & -1818 & -5769 & 10222 & -916 & -6117 & 2534 & -10284 \\ -1229 & 1820 & -674 & 0 & 2154 & -753 & -2041 & 0 & -171 & -2882 & 1049 & 0 \\ 1229 & -2154 & 171 & 2243 & -1820 & 753 & 2882 & -10222 & 674 & 2041 & -1049 & 10284 \end{pmatrix}$$

$$Q_8^5 := \begin{pmatrix} 11906 & -19141 & 4633 & 9663 & -19141 & 7289 & 22241 & -44205 & 4633 & 22241 & -9810 & 45666 \\ 6143 & -8801 & 2198 & 2230 & -10667 & 3179 & 11292 & -7843 & 1316 & 13998 & -4854 & 4748 \\ -2077 & 3980 & -1461 & -2256 & 3312 & -2436 & -2714 & 12602 & -2466 & -1032 & 2201 & -15821 \\ -2250 & 3373 & -859 & -1169 & 4295 & -1963 & -4001 & 5154 & -1398 & -4328 & 2314 & -3992 \\ 35 & 48 & 551 & -1169 & 48 & 16 & -1532 & 5154 & 551 & -1532 & 328 & -3992 \\ -2250 & 4295 & -1398 & -2256 & 3373 & -1963 & -4328 & 12602 & -859 & -4001 & 2314 & -15821 \\ -2077 & 3312 & -2466 & 2230 & 3980 & -2436 & -1032 & -7843 & -1461 & -2714 & 2201 & 4748 \\ 6143 & -10667 & 1316 & 9663 & -8801 & 3179 & 13998 & -44205 & 2198 & 11292 & -4854 & 45666 \end{pmatrix}$$

$$Q_9^4 := \begin{pmatrix} 3183 & -4720 & 270 & 3966 & -4632 & 573 & 7101 & -14962 & 462 & 6962 & -2341 & 12961 \\ 3183 & -4632 & 462 & 3038 & -4720 & 573 & 6962 & -11462 & 270 & 7101 & -2341 & 9929 \\ 1694 & -2376 & 437 & 688 & -2599 & 305 & 3565 & -2598 & -47 & 3917 & -1245 & 2250 \\ -588 & 990 & 208 & -1983 & 737 & -106 & -1499 & 7481 & -343 & -1099 & 432 & -6480 \\ -2595 & 3894 & -118 & -3727 & 3729 & -467 & -5862 & 14060 & -478 & -5602 & 1908 & -12179 \\ -3388 & 4976 & -389 & -3727 & 4976 & -610 & -7483 & 14060 & -389 & -7483 & 2491 & -12179 \\ -2595 & 3729 & -478 & -1983 & 3894 & -467 & -5602 & 7481 & -118 & -5862 & 1908 & -6480 \\ -588 & 737 & -343 & 688 & 990 & -106 & -1099 & -2598 & 208 & -1499 & 432 & 2250 \\ 1694 & -2599 & -47 & 3038 & -2376 & 305 & 3917 & -11462 & 437 & 3565 & -1245 & 9929 \end{pmatrix}$$

$$Q_9^5 := \begin{pmatrix} 14017 & -20354 & 1967 & 13664 & -20354 & 2062 & 30248 & -51185 & 1967 & 30248 & -12462 & 44620 \\ 7903 & -10773 & 1567 & 3614 & -12119 & 1014 & 16832 & -12665 & -54 & 18097 & -5800 & 9676 \\ -2098 & 3564 & -396 & -3759 & 2728 & -716 & -4165 & 15361 & -1761 & -3145 & 4473 & -15149 \\ -3927 & 5626 & -979 & -2220 & 6116 & -1074 & -8068 & 9019 & -1058 & -8089 & 4665 & -8269 \\ 356 & -565 & 123 & 455 & -56 & -383 & 403 & -1473 & 381 & 158 & -1804 & 1848 \\ 356 & -56 & 381 & -2220 & -565 & -383 & 158 & 9019 & 123 & 403 & -1804 & -8269 \\ -3927 & 6116 & -1058 & -3759 & 5626 & -1074 & -8089 & 15361 & -979 & -8068 & 4665 & -15149 \\ -2098 & 2728 & -1761 & 3614 & 3564 & -716 & -3145 & -12665 & -396 & -4165 & 4473 & 9676 \\ 7903 & -12119 & -54 & 13664 & -10773 & 1014 & 18097 & -51185 & 1567 & 16832 & -5800 & 44620 \end{pmatrix}$$

$$Q_{10}^4 := \begin{pmatrix} 3134 & -4322 & -176 & 4267 & -4264 & -258 & 7200 & -14386 & -21 & 7174 & -1768 & 11387 \\ 3134 & -4264 & -21 & 3452 & -4322 & -258 & 7174 & -11639 & -176 & 7200 & -1768 & 9212 \\ 1937 & -2578 & 141 & 1318 & -2729 & -159 & 4408 & -4445 & -263 & 4476 & -1093 & 3518 \\ 0 & 93 & 250 & -1318 & -93 & 0 & -42 & 4445 & -250 & 42 & 0 & -3518 \\ -1937 & 2729 & 263 & -3452 & 2578 & 159 & -4476 & 11639 & -141 & -4408 & 1093 & -9212 \\ -3134 & 4322 & 176 & -4267 & 4264 & 258 & -7200 & 14386 & 21 & -7174 & 1768 & -11387 \\ -3134 & 4264 & 21 & -3452 & 4322 & 258 & -7174 & 11639 & 176 & -7200 & 1768 & -9212 \\ -1937 & 2578 & -141 & -1318 & 2729 & 159 & -4408 & 4445 & 263 & -4476 & 1093 & -3518 \\ 0 & -93 & -250 & 1318 & 93 & 0 & 42 & -4445 & 250 & -42 & 0 & 3518 \\ 1937 & -2729 & -263 & 3452 & -2578 & -159 & 4476 & -11639 & 141 & 4408 & -1093 & 9212 \end{pmatrix}$$

$$Q_{10}^5 := \begin{pmatrix} 14143 & -19112 & -251 & 15685 & -19112 & -1732 & 32197 & -52248 & -251 & 32197 & -10643 & 41144 \\ 8913 & -11597 & 480 & 5547 & -12500 & -1114 & 20374 & -18177 & -1196 & 20460 & -5557 & 13768 \\ -744 & 1403 & 306 & -3666 & 636 & -15 & -1463 & 12820 & -1289 & -1315 & 3348 & -11019 \\ -4619 & 6281 & -260 & -3995 & 6372 & 304 & -10353 & 13992 & -477 & -10195 & 5534 & -11694 \\ -1230 & 1603 & -314 & 244 & 2087 & -277 & -2894 & -196 & 241 & -2791 & 166 & -54 \\ 1604 & -1937 & 145 & 244 & -1937 & -697 & 3446 & -196 & 145 & 3446 & -3569 & -54 \\ -1230 & 2087 & 241 & -3995 & 1603 & -277 & -2791 & 13992 & -314 & -2894 & 166 & -11694 \\ -4619 & 6372 & -477 & -3666 & 6281 & 304 & -10195 & 12820 & -260 & -10353 & 5534 & -11019 \\ -744 & 636 & -1289 & 5547 & 1403 & -15 & -1315 & -18177 & 306 & -1463 & 3348 & 13768 \\ 8913 & -12500 & -1196 & 15685 & -11597 & -1114 & 20460 & -52248 & 480 & 20374 & -5557 & 41144 \end{pmatrix}$$

Appendix: K and T for special rules 6 and 7

For $n=3,5,\dots,10$, the tables

$$T_n := 10^5 \begin{pmatrix} \tau_{11,2} & \tau_{11,3} & \tau_{11,4} & \tau_{11,5} & \tau_{11,6} \\ \tau_{22,2} & \tau_{22,3} & \tau_{22,4} & \tau_{22,5} & \tau_{22,6} \\ \tau_{21,2} & \tau_{21,3} & \tau_{21,4} & \tau_{21,5} & \tau_{21,6} \\ \tau_{12,2} & \tau_{12,3} & \tau_{12,4} & \tau_{12,5} & \tau_{12,6} \\ \tau_{31,2} & \tau_{31,3} & \tau_{31,4} & \tau_{31,5} & \tau_{31,6} \\ \tau_{32,2} & \tau_{32,3} & \tau_{32,4} & \tau_{32,5} & \tau_{32,6} \end{pmatrix}.$$

encode the stencil weights $\tau_{ij,k}$, where $_{ij}$ indicates the location of refined node $\tilde{\mathbf{d}}^s_{ij}$ in sector s and $_k$ labels the weights of the quadratic expansion coefficient $\mathbf{q}^s_k$.

For the tables K see Fig. 18. Fig. 18a displays K consisting of the four groups κ^r_{ij}, $r=-1,0,1,2$ in formulas (6) and (7) arranged around a filler $\mathbf{0}$ in the center. Since even in this compact grouping many weights κ^r_{ij} (scaled by 10^5) are 0, we focus on pieces of K. For $l=1,2$, Fig. 18b displays the only nonzero 5×5 matrices K^n_{lm}, where lm , $m=1,2$ is the index of the refined node $\tilde{\mathbf{d}}^s_{lm}$. For $l=3$, Fig. 18c shows the only nonzero entries dark and light underlaid. The weights are symmetric across the center line so that only the left (darker underlaid) 5×4 matrices K^n_{3m}, $m=1,2$, are given.

$$K^3_{11} := \begin{pmatrix} 0 & 0 & -61 & 54 & 0 & 0 & -256 & 1016 & 0 & 0 & -1273 & 1980 \\ -1 & -17 & -31 & 54 & -17 & 1715 & 9345 & 1016 & -31 & 9345 & 45137 & 1980 \\ 0 & 0 & 0 & 0 & 0 & 0 & 0 & 0 & -61 & -256 & -1273 & 0 \end{pmatrix}$$

$$K^3_{22} := \begin{pmatrix} 0 & 0 & -48 & -86 & 0 & 0 & -1312 & -1294 & 0 & 0 & -3426 & -1910 \\ 0 & 0 & -30 & -86 & 0 & -4 & 12 & -1294 & -30 & 12 & 3064 & -1910 \\ 0 & 0 & 0 & 0 & 0 & 0 & 0 & 0 & -48 & -1312 & -3426 & 0 \end{pmatrix}$$

$$K^3_{21} := \begin{pmatrix} 0 & 0 & -58 & -159 & 0 & 0 & -1793 & -2228 & 0 & 0 & -4669 & -2486 \\ 0 & -8 & 30 & -25 & -5 & 171 & 6171 & 3663 & -160 & 390 & 22303 & 9973 \\ 0 & 0 & 0 & 0 & 0 & 0 & 0 & 0 & -149 & -1335 & -2753 & 0 \end{pmatrix}$$

$$K^3_{12} := \begin{pmatrix} 0 & 0 & -149 & -25 & 0 & 0 & -1335 & 3663 & 0 & 0 & -2753 & 9973 \\ 0 & -5 & -160 & -159 & -8 & 171 & 390 & -2228 & 30 & 6171 & 22303 & -2486 \\ 0 & 0 & 0 & 0 & 0 & 0 & 0 & 0 & -58 & -1793 & -4669 & 0 \end{pmatrix}$$

$$K^3_{31} := \begin{pmatrix} 0 & 0 & 29 & 79 & 0 & 0 & 896 & 1114 & 29 & 896 & 4669 & 1243 \\ 0 & 4 & 83 & 74 & 2 & -85 & 1433 & 4037 & 80 & -195 & -974 & 7627 \\ 0 & 2 & 80 & 79 & 4 & -85 & -195 & 1114 & 83 & 1433 & -974 & 1243 \end{pmatrix}$$

$$K^3_{32} := \begin{pmatrix} 0 & 0 & 24 & 43 & 0 & 0 & 656 & 647 & 24 & 656 & 3426 & 955 \\ 0 & 0 & 37 & 83 & 0 & 2 & -124 & -254 & 15 & -6 & -1365 & -1182 \\ 0 & 0 & 15 & 43 & 0 & 2 & -6 & 647 & 37 & -124 & -1365 & 955 \end{pmatrix}$$

$$T_3 := \begin{pmatrix} -6513 & 17123 & -6513 & 22618 & 17123 \\ -15573 & 49756 & -15573 & 38712 & 49756 \\ -21775 & 46294 & -9757 & -826 & 53690 \\ -9757 & 53690 & -21775 & -826 & 46294 \\ 138882 & -46294 & 189605 & -46294 & 24731 \\ 149268 & -49756 & 204560 & -49756 & -15366 \end{pmatrix}$$

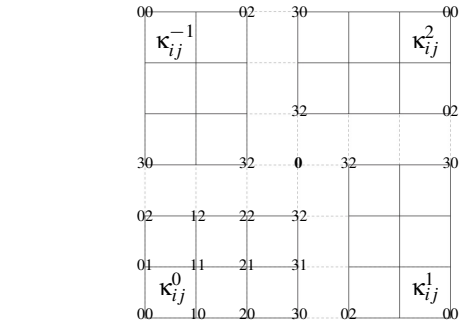

(a) *labels of coefficients* κ_{ij}^{k}

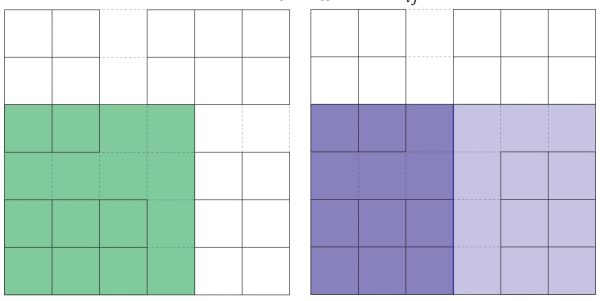

(b) 5×5*:* K_{11}^n, K_{21}^n, K_{12}^n, K_{22}^n. **(c)** 5×4*:* K_{31}^n *and* K_{32}^n

Figure 18: *Structure of matrices* K^n, $n>4$. *(a) Labels of all coefficients* κ_{ij}^k, $i=0,\ldots,3$, $j=0,1,2$, $k=-1,0,1,2$. *(b)* K_{11}^n, K_{21}^n, K_{12}^n, K_{22}^n. *(c) (*left *darker):* K_{31}^n *and* K_{32}^n.

$$K_{11}^5:=\begin{pmatrix}-23&25&-1375&0&0\\7&2707&4721&0&0\\77&7200&57124&4721&-1375\\0&2722&7200&2707&25\\-17&0&77&7&-23\end{pmatrix},\ K_{22}^5:=\begin{pmatrix}-69&578&-1827&0&0\\-53&456&2700&0&0\\173&-1206&22655&2700&-1827\\10&-12&-1206&456&578\\-1&10&173&-53&-69\end{pmatrix}$$

$$K_{21}^5:=\begin{pmatrix}2&11&-601&0&0\\-77&773&902&0&0\\162&-1193&38518&16370&-316\\55&-189&7137&4468&1650\\0&-4&50&-28&-104\end{pmatrix},\ K_{12}^5:=\begin{pmatrix}-104&1650&-316&0&0\\-28&4468&16370&0&0\\50&7137&38518&902&-601\\-4&-189&-1193&773&11\\0&55&162&-77&2\end{pmatrix}$$

$$K_{31}^5:=\begin{pmatrix}-1&-5&300&0\\38&-386&-451&0\\-81&596&5913&33658\\-27&94&2134&8588\\0&2&-16&-56\end{pmatrix},\ K_{32}^5:=\begin{pmatrix}34&-289&913&0\\26&-228&-1350&0\\-86&603&-4644&8840\\-5&6&581&79\\0&-5&-69&19\end{pmatrix}$$

$$T_5:=\begin{pmatrix}-2527&7380&-2527&3320&7380\\5551&17986&5551&29927&17986\\437&1272&-6216&12934&24686\\-6216&24686&437&12934&1272\\1758&-1272&6438&786&38034\\24856&-17986&29236&11116&52248\end{pmatrix}$$

$$K_{11}^6:=\begin{pmatrix}18&4&-1758&0&0\\-213&4243&3816&0&0\\338&4608&60313&3816&-1758\\-66&4510&4608&4243&4\\-71&-66&338&-213&18\end{pmatrix},\ K_{22}^6:=\begin{pmatrix}-134&881&-1751&0&0\\-183&1012&2753&0&0\\438&-2681&28732&2753&-1751\\13&115&-2681&1012&881\\-6&13&438&-183&-134\end{pmatrix}$$

$$K_{21}^6:=\begin{pmatrix}53&-109&-597&0&0\\-243&1557&456&0&0\\339&-2339&42089&17527&-261\\108&-193&6916&4270&2229\\-2&-13&107&0&-252\end{pmatrix},\ K_{12}^6:=\begin{pmatrix}-252&2229&-261&0&0\\0&4270&17527&0&0\\107&6916&42089&456&-597\\-13&-193&-2339&1557&-109\\-2&108&339&-243&53\end{pmatrix}$$

$$K_{31}^6:=\begin{pmatrix}-26&54&298&0\\121&-778&-228&0\\-169&1169&7905&40111\\-54&96&1655&8187\\1&6&35&-75\end{pmatrix},\ K_{32}^6:=\begin{pmatrix}67&-440&875&0\\91&-506&-1376&0\\-219&1340&-4166&15895\\-6&-57&963&-885\\3&-6&-155&177\end{pmatrix}$$

$$T_6:=\begin{pmatrix}-2416&8465&-2416&399&8465\\5841&15223&5841&28835&15223\\1336&279&-5771&10537&22308\\-5771&22308&1336&10537&279\\279&-279&5628&279&28911\\15223&-15223&23834&15223&47863\end{pmatrix}$$

$$K_{11}^7:=\begin{pmatrix}79&67&-2261&0&0\\-571&5727&2892&0&0\\707&2372&62007&2892&-2261\\-198&6316&2372&5727&67\\-136&-198&707&-571&79\end{pmatrix},\ K_{22}^7:=\begin{pmatrix}-182&1097&-1873&0&0\\-358&1653&2438&0&0\\720&-4032&32922&2438&-1873\\-1&345&-4032&1653&1097\\-11&-1&720&-358&-182\end{pmatrix},$$

$$K_{21}^7:=\begin{pmatrix}116&-195&-717&0&0\\-443&2259&21&0&0\\515&-3253&44307&18253&-283\\140&-96&6620&4151&2646\\-9&-22&156&40\end{pmatrix},\ K_{12}^7:=\begin{pmatrix}-390&2646&-283&0&0\\40&4151&18253&0&0\\156&6620&44307&21&-717\\-22&-96&-3253&2259&-195\\-9&140&515&-443&116\end{pmatrix}$$

$$K_{31}^7:=\begin{pmatrix}-58&97&358&0\\221&-1129&-10&0\\-257&1626&9214&44198\\-70&48&1214&7545\\4&11&106&-62\end{pmatrix},\ K_{32}^7:=\begin{pmatrix}91&-548&936&0\\179&-826&-1219&0\\-360&2016&-3499&21611\\0&-172&1162&-2264\\5&0&-236&424\end{pmatrix},$$

$$T_7:=\begin{pmatrix}-3023&10233&-3023&-1398&10233\\5479&14409&5479&27892&14409\\1392&445&-5564&8885&21086\\-5564&21086&1392&8885&445\\335&-445&4914&555&23157\\10850&-14409&22750&17968&42010\end{pmatrix}$$

$$K_{11}^8:=\begin{pmatrix}133&180&-2734&0&0\\-954&6990&2104&0&0\\1092&619&62877&2104&-2734\\-357&7894&619&6990&180\\-195&-357&1092&-954&133\end{pmatrix},\ K_{22}^8:=\begin{pmatrix}-219&1275&-2056&0&0\\-544&2275&2040&0&0\\981&-5149&35835&2040&-2056\\-27&604&-5149&2275&1275\\-15&-27&981&-544&-219\end{pmatrix}$$

$$K_{21}^8:=\begin{pmatrix}174&-245&-850&0&0\\-636&2835&-329&0&0\\673&-3944&45740&18733&-326\\154&30&6345&4083&2957\\-17&-31&197&76&-505\end{pmatrix},\ K_{12}^8:=\begin{pmatrix}-505&2957&-326&0&0\\76&4083&18733&0&0\\197&6345&45740&-329&-850\\-31&30&-3944&2835&-245\\-17&154&673&-636&174\end{pmatrix}$$

$$K_{31}^8:=\begin{pmatrix}-87&122&425&0\\318&-1417&164&0\\-336&1972&10117&46915\\-77&-15&858&6937\\8&15&174&-36\end{pmatrix},\ K_{32}^8:=\begin{pmatrix}109&-637&1028&0\\272&-1137&-1020&0\\-490&2574&-2852&26033\\13&-302&1250&-3649\\7&13&-304&697\end{pmatrix}$$

$$T_8:=\begin{pmatrix}-3737&11875&-3737&-2513&11875\\4990&14315&4990&27137&14315\\1234&838&-5462&7767&20385\\-5462&20385&1234&7767&838\\491&-838&4452&1186&19155\\8386&-14315&23016&20245&36486\end{pmatrix}$$

$$K_{11}^9:=\begin{pmatrix}176&307&-3135&0&0\\-1310&8019&1465&0&0\\1446&-718&63315&1465&-3135\\-517&9198&-718&8019&307\\-245&-517&1446&-1310&176\end{pmatrix},\ K_{22}^9:=\begin{pmatrix}-248&1425&-2244&0&0\\-718&2829&1658&0&0\\1207&-6040&37908&1658&-2244\\-59&851&-6040&2829&1425\\-18&-59&1207&-718&-248\end{pmatrix}$$

$$K_{21}^9:=\begin{pmatrix}222&-272&-967&0&0\\-806&3292&-600&0&0\\809&-4463&46706&19065&-371\\157&154&6115&4045&3194\\-25&-40&231&105&-599\end{pmatrix},\ K_{12}^9:=\begin{pmatrix}-599&3194&-371&0&0\\105&4045&19065&0&0\\231&6115&46706&-600&-967\\-40&154&-4463&3292&-272\\-25&157&809&-806&222\end{pmatrix}$$

$$K_{31}^9:=\begin{pmatrix}-111&136&483&0\\403&-1646&300&0\\-404&2231&10765&48801\\-78&-77&579&6424\\12&20&232&-7\end{pmatrix},\ K_{32}^9:=\begin{pmatrix}124&-712&1122&0\\359&-1414&-829&0\\-603&3020&-2288&29428\\29&-425&1278&-4887\\9&29&-359&957\end{pmatrix}$$

$$T_9:=\begin{pmatrix}-4380&13232&-4380&-3232&13232\\4527&14476&4527&26550&14476\\1040&1226&-5409&6991&19945\\-5409&19945&1040&6991&1226\\573&-1226&4235&1878&16211\\6773&-14476&23771&22179&31709\end{pmatrix}$$

$$K_{11}^{10}:=\begin{pmatrix}208&431&-3466&0&0\\-1620&8844&954&0&0\\1753&-1740&63528&954&-3466\\-664&10255&-1740&8844&431\\-284&-664&1753&-1620&208\end{pmatrix},\ K_{22}^{10}:=\begin{pmatrix}-272&1553&-2414&0&0\\-872&3303&1323&0&0\\1396&-6746&39421&1323&-2414\\-92&1070&-6746&3303&1553\\-19&-92&1396&-872&-272\end{pmatrix}$$

$$K_{21}^{10}:=\begin{pmatrix}261&-285&-1065&0&0\\-950&3652&-809&0&0\\923&-4855&47384&19304&-412\\154&265&5928&4022&3377\\-32&-48&258&127&-674\end{pmatrix},\ K_{12}^{10}:=\begin{pmatrix}-674&3377&-412&0&0\\127&4022&19304&0&0\\258&5928&47384&-809&-1065\\-48&265&-4855&3652&-285\\-32&154&923&-950&261\end{pmatrix}$$

$$K_{31}^{10}:=\begin{pmatrix}-130&142&532&0\\475&-1826&404&0\\-461&2427&11246&50160\\-77&-132&361&6007\\16&24&281&20\end{pmatrix},\ K_{32}^{10}:=\begin{pmatrix}136&-776&1207&0\\436&-1651&-661&0\\-698&3373&-1813&32055\\46&-535&1277&-5942\\9&46&-403&1189\end{pmatrix}$$

$$T_{10}:=\begin{pmatrix}-4918&14316&-4918&-3714&14316\\4128&14713&4128&26095&14713\\860&1556&-5380&6436&19652\\-5380&19652&860&6436&1556\\594&-1556&4178&2519&13975\\5620&-14713&24674&23806&27708\end{pmatrix}$$